Axial acoustic radiation torque of a Bessel vortex beam on spherical shells

F. G. Mitri*
Los Alamos National Laboratory, MPA-11, Sensors & Electrochemical Devices, Acoustics & Sensors Technology Team, MS D429, Los Alamos, New Mexico 87545, USA

T. P. Lobo and G. T. Silva
Instituto de Física, Universidade Federal de Alagoas, Maceió, Alagoas 57072-970, Brasil
(Received 6 October 2011; revised manuscript received 7 January 2012; published 15 February 2012)

The present paper investigates the interaction of an acoustic Bessel vortex beam centered on a viscoelastic polyethylene sphere and spherical shells filled with air or water immersed in nonviscous water and mercury, and the induced axial acoustic radiation torque (ART) resulting from the transfer of angular momentum. Closed-form series expansions for the axial ART are derived for the case of progressive, standing, and quasistanding waves. The ART is shown to be the result of acoustic absorption inside the particle's material. Numerical predictions shown in the form of two-dimensional (2D) plots illustrate the theory, and reveal new properties related to the ART of Bessel vortex beams. Potential applications are in particle rotation and manipulation. Other applications, such as the characterization of fluids from induced angular accelerations (produced by the ART) and containerless processing, may benefit from the analysis developed here.

DOI: 10.1103/PhysRevE.85.026602 PACS number(s): 43.25.Qp, 43.20.Fn, 43.20.Ks

I. INTRODUCTION

Physicists and engineers are familiar with the fact that the transfer of (linear) momentum from electromagnetic [1] and acoustical [2] propagating waves upon reflection or absorption from a particle induces forces that may be used under various circumstances to accelerate [3], trap [4,5], levitate [6], or even stretch [7] the particle itself. Furthermore, the transfer of *angular* momentum [8] induces a radiation torque responsible for rotating particles [9,10]. In acoustics, a particular type of sound beams, known as acoustical vortices [11], have been realized experimentally [12,13] and correspond to vortex (or spiral, helicoidal, corkscrew) waves that carry an orbital angular momentum [13–15] and the induced torque set the particles into well-controlled rotations [16].

Quantitative theoretical analyses and numerical simulations allowing the estimation of the acoustic radiation torque exist in the literature [17–20], which are of particular importance for experimental design purposes. Numerical simulations are more practical to build in a shorter amount of time and predictions can be effective in showing new emergent phenomena related to particle rotation of any size using a vortex beam. In those studies [17–20], however, the numerical predictions for the radiation torque involved the interaction of an incident plane wave with the target under consideration, and the torque expression presented in Ref. [20] is *only* valid for a scatterer much smaller than the wavelength of the sound wave. On the other hand, when the acoustic illumination is in the form of a localized acoustic beam (such as a vortex beam), it is anticipated that the torque will depend on the beam's parameters (order of helicity, and half-conical angle).

An example of a vortex beam includes the Bessel (vortex) beam of any order (or topological charge) $|m| \geqslant 1$ [21], which has been investigated from the standpoint of acoustic scattering [22–24] and radiation force [25–28] theories. Because a Bessel vortex beam carries orbital angular momentum [29], it can induce rotation of a particle depending on its mechanical properties and position within the acoustic field. Nevertheless, this phenomenon cannot be achieved using plane waves because of symmetry considerations.

In view of the prominent applications of vortex beams and their advantageous features and characteristics, it is of some importance to work out the theoretical development from the standpoint of acoustic radiation torque theory, though preliminary studies have been recently available [30,31]. In this work a closed-form expression for the radiation torque experienced by a viscoelastic spherical shell of *any* size and *centered* on the axis of the incident acoustic beam of quasistanding waves is provided. It is also shown that additional closed-form expressions for the case of standing and progressive waves can be obtained with appropriate choice of the beam's parameters. Numerical predictions of the axial radiation torque are presented for polyethylene (PE) viscoelastic shells immersed in nonviscous fluids with particular emphasis on their relative thickness, the internal fluid that fills their hollow region, and the outer surrounding fluid. Several features of these theoretical results can be related to experiments yet to be designed, and the analytical solution can potentially serve as a benchmark for comparison to other results obtained using finite-element models or by strictly numerical or asymptotic approaches in the applied field of particle manipulation, mixing, and rotation. It is important to emphasize that the ability to rotate objects offers a new degree of control in optics [32] and fluid mechanics [33], and is expected to have significant applications in the areas of acoustic manipulation [34] and biotechnology at the microscale. For example, this could lead to the development of a new type of biological micromachines using acoustical waves.

II. AXIAL RADIATION TORQUE

Consider a monofrequency acoustical Bessel vortex beam of quasistanding waves [26] incident upon a spherical scatterer submerged in a nonviscous (ideal) fluid. In an ideal fluid there is no absorption of linear and/or angular momentum,

*mitri@lanl.gov

therefore the acoustic radiation torque can be evaluated from the integration over a control sphere of surface S_R with large radius enclosing the scatterer (i.e., in the far field from the scatterer). Physically, this means that the mean angular momentum change in a unit time which occurs inside the surface at large radius in the far field entirely goes into the torque experienced by the particle.

Based on the conservation law of angular momentum, the time-averaged acoustic radiation torque (ART) exerted on an object immersed in an ideal fluid is evaluated by integrating the moment of the time-averaged (Brillouin) radiation stress tensor over any spherical surface enclosing it as [17,20]

$$\langle \mathbf{N} \rangle = \iint_{S_R} \mathbf{r} \times \langle \mathbf{\Pi} \rangle d\mathbf{S_R}, \tag{1}$$

where the symbol $\langle \cdot \rangle$ denotes time averaging over a period of the acoustical waves, $\mathbf{r}$ is the vector position from the center of the control sphere to a point in space, $d\mathbf{S_R} = \mathbf{n}\, dS_R$is the differential surface with $\mathbf{n}$ the outward normal to it, and the time-averaged radiation stress tensor is expressed as [35]

$$\langle \mathbf{\Pi} \rangle = (\langle K \rangle - \langle V \rangle)\mathbf{I} - \rho_0 \langle \mathbf{vv} \rangle. \tag{2}$$

In Eq. (2) $\mathbf{I}$ is the second-rank unit tensor in $\mathbb{R}^3$, $\langle K \rangle = \frac{\rho_0}{2} \langle v^{(1)^2} \rangle \cdot$ is the time-averaged kinetic energy density, $\langle V \rangle = \frac{\langle p^{(1)^2} \rangle}{2\rho_0 c_0^2}$ is the time-averaged potential energy density, $\mathbf{v} = \nabla \Phi$ is the fluid particle velocity vector where Φ is the velocity potential, and p is the pressure. The superscript (1) denotes quantities in the linear (first order) approximation.

Upon the substitution of Eq. (2) into Eq. (1), the time-averaged ART can be expressed as

$$\langle \mathbf{N} \rangle = \iint_{S_R} \mathbf{r} \times \left[\left(\frac{\rho_0}{2} \langle v^{(1)^2} \rangle - \frac{\langle p^{(1)^2} \rangle}{2\rho_0 c_0^2} \right) \mathbf{n} - \rho_0 \langle \mathbf{v} v_n^{(1)} \rangle \right] dS_R, \tag{3}$$

where $v_n^{(1)} = \mathbf{v} \cdot \mathbf{n}$ is the normal velocity.

Equation (3) can be further simplified by noticing that $\mathbf{r} \times \mathbf{n} = 0$ on the surface of the virtual sphere enclosing the object. Thus, the expression for the ART in the far field can be reduced to [17]

$$\langle \mathbf{N} \rangle = -\rho_0 \iint_{S_R} \left\langle v_n^{(1)} (\mathbf{r} \times \mathbf{v}) \right\rangle dS_R. \tag{4}$$

Using the properties for the time average of the product of two complex numbers, where the superscript * denotes a complex conjugate, the axial component (i.e., in the direction of wave propagation) of the ART can be rewritten in terms of the total (incident + scattered) velocity potential as

$$\langle N_z \rangle = \langle \mathbf{N} \rangle \cdot \mathbf{e}_z = \frac{\rho_0}{2} \mathrm{Im} \left\{ \iint_{S_R} \frac{\partial \Phi^*}{\partial r} \hat{L}_z \Phi \, dS_R \right\}, \tag{5}$$

where $\mathbf{e}_z$ is the unitary vector along the axial direction, and $\hat{L}_z$ is the axial component of the angular momentum operator given by [36]

$$\hat{L}_z = -i \frac{\partial}{\partial \phi}. \tag{6}$$

To further simplify the expression given by Eq. (5), the *asymptotic* forms ($kr \to \infty$) of the total velocity potential $\Phi (= \Phi^{(\mathrm{inc})}_{J_m,\mathrm{qst}} + \Phi^{(\mathrm{sc})}_{J_m,\mathrm{qst}})$ are used. For a spherical target in the field of an acoustical Bessel vortex beam of quasistanding waves, the incident velocity potential is expressed as [26]

$$\Phi^{(\mathrm{inc})}_{J_m,\mathrm{qst}} = e^{-i\omega t} \frac{1}{kr} \sum_{n=|m|}^{\infty} \left\{ \frac{(n-m)!}{(n+m)!} (2n+1) i^{(n-m)} \times \sin\left(kr - \frac{n\pi}{2} \right) [\Phi_0 e^{ik_z h} + \Phi_1 (-1)^n e^{-ik_z h}] \times P_n^m(\cos\theta) P_n^m(\cos\beta) e^{im\phi} \right\}, \tag{7}$$

and the scattered field is given by [26]

$$\Phi^{(\mathrm{sc})}_{J_m,\mathrm{qst}} = \frac{e^{-i(\omega t - kr)}}{kr} \sum_{n=|m|}^{\infty} \left\{ \frac{(n-m)!}{(n+m)!} (2n+1) i^{-(m+1)} \times A_n(ka) [\Phi_0 e^{ik_z h} + \Phi_1 (-1)^n e^{-ik_z h}] \times P_n^m(\cos\theta) P_n^m(\cos\beta) e^{im\phi} \right\}, \tag{8}$$

with the assumption that the amplitude $|\Phi_0| \geqslant |\Phi_1|$. The parameter $k_z = k \cos\beta$ is the axial wave number, $k = \omega/c = 2\pi/\lambda$ is defined as the wave number of the incident Bessel vortex beam, ω is the angular frequency, c_0 is the speed of sound in the fluid medium with a density denoted by ρ_0, the parameter λ being the wavelength of the acoustic radiation making up the beam, β is the half-cone angle formed by the wave-number k relative the axis of wave propagation, h is the distance in the z direction from the center of the sphere to the nearest velocity potential antinode, the angle θ is the scattering angle relative to the beam axis of wave propagation z, $P_n^m(\cdot)$ are the associated Legendre functions, and m is the order (or helicity) of the beam. The dimensionless (complex) scattering coefficients $A_n(ka) = (\alpha_n + i\beta_n)$ in Eq. (8) are determined from appropriate boundary conditions at the surface of the sphere. Note also that for $m = 0$ and $\beta = 0\,^\circ$, the case of plane (standing or quasistanding) waves [37,38] can be recovered from Eqs. (7) and (8).

The substitution of the total field Φ into Eq. (5) using the property for the axial component of the angular momentum operator (Eq. (26) in Ref. [18]),

$$\iint_{S_R} f_1 \hat{L}_z f_2 \, dS_R = -\iint_{S_R} f_2 \hat{L}_z f_1 \, dS_R \tag{9}$$

leads to a simplified expression for the ART in terms of the incident and scattered velocity potentials such that

$$\langle N_z \rangle = \frac{\rho_0}{2} \mathrm{Im} \left\{ \iint_{S_R} \left(\frac{\partial \Phi^{(\mathrm{inc})^*}_{J_m,\mathrm{qst}}\big|_{kr\to\infty}}{\partial r} - ik \Phi^{(\mathrm{inc})^*}_{J_m,\mathrm{qst}}\big|_{kr\to\infty} - ik \Phi^{(\mathrm{sc})^*}_{J_m,\mathrm{qst}}\big|_{kr\to\infty} \right) \hat{L}_z \Phi^{(\mathrm{sc})}_{J_m,\mathrm{qst}}\big|_{kr\to\infty} \, dS_R \right\}. \tag{10}$$

After substituting Eqs. (7) and (8) into Eq. (10) and manipulating the result using the properties of the associated Legendre functions (see Eqs. (5) and (9) in Ref. [39]), the axial component of the ART expression can be reduced to

$$\langle N_z \rangle = \pi a^3 E_0 \tau_z^{\mathrm{qst}}(m, ka, \beta), \tag{11}$$

where a is the radius of the sphere, $E_0 = \frac{\rho_0 k^2 |\Phi_0|^2}{2}$ is a characteristic energy density, and the dimensionless axial component τ_z^{qst} is found to be

$$\tau_z^{\mathrm{qst}}(m,ka,\beta) = -\frac{4m}{(ka)^3}\sum_{n=|m|}^{\infty}\left\{P_n^m(\cos\beta)^2(2n+1) \times \frac{(n-m)!}{(n+m)!}\left(\alpha_n+\alpha_n^2+\beta_n^2\right)\left[1+\frac{|\Phi_1|^2}{|\Phi_0|^2} + 2(-1)^n\frac{|\Phi_1|}{|\Phi_0|}\cos(2kh\cos\beta)\right]\right\}. \quad (12)$$

Equation (12) is the general closed-form expression for the dimensionless axial ART in a Bessel vortex beam of quasistanding waves. When $|\Phi_1| = |\Phi_0|$,the incident beam corresponds to an equiamplitude standing wave field, and the expression for the axial dimensionless torque τ_z^{st} is given by

$$\tau_z^{\mathrm{st}}(m,ka,\beta) = -\frac{8m}{(ka)^3}\sum_{n=|m|}^{\infty}\left\{P_n^m(\cos\beta)^2(2n+1) \times \frac{(n-m)!}{(n+m)!}\left(\alpha_n+\alpha_n^2+\beta_n^2\right) \times\left[1+(-1)^n\cos(2kh\cos\beta)\right]\right\}. \quad (13)$$

Furthermore, when $|\Phi_1| = 0$, the incident beam corresponds to a progressive (or travelling) wave field, and the expression for the axial dimensionless torque τ_z^p is

$$\tau_z^p(m,ka,\beta) = -\frac{4m}{(ka)^3}\sum_{n=|m|}^{\infty}\left\{P_n^m(\cos\beta)^2(2n+1) \times \frac{(n-m)!}{(n+m)!}\left(\alpha_n+\alpha_n^2+\beta_n^2\right)\right\}. \quad (14)$$

From Eqs. (12)–(14) it is important to note the dependence of the axial dimensionless torque on the order m of the beam; it can be easily noticed that $\tau_z(-m,ka,\beta) = -\tau_z(m,ka,\beta)$ so that the dimensionless axial ART reverses sign when the beam reverses its handedness. Furthermore, when $m = 0$, which corresponds to the fundamental zeroth-order Bessel beam, the torque vanishes, as well as in the case of plane waves (i.e., $m = 0$ and $\beta = 0^\circ$).

Moreover, a particular attention is given to the term

$$\Gamma_n = \left(\alpha_n+\alpha_n^2+\beta_n^2\right). \quad (15)$$

After arithmetic manipulation, Γ_n is rewritten in terms of the scattering coefficients $A_n(ka) = (\alpha_n + i\beta_n)$ as

$$\Gamma_n = \mathrm{Re}\{A_n(ka)\} + |A_n(ka)|^2. \quad (16)$$

From the formalism of the resonance scattering theory [40], the scattering coefficients $A_n(ka)$ may be rewritten in terms of a scattering function S_n, such that

$$S_n = 2A_n(ka) + 1 = (2\alpha_n + 1 + 2i\beta_n). \quad (17)$$

For perfectly rigid, fluid, and elastic materials in which the assumption of no absorption holds, the modulus of the scattering function equals unity (see Eq. (21), p. 200, in Ref. [40]). From Eq. (17) it is straightforward to show that

$$\frac{|S_n|-1}{4} = \mathrm{Re}\{A_n(ka)\} + |A_n(ka)|^2 = \Gamma_n = 0. \quad (18)$$

Therefore, as shown from Eq. (18), the torque vanishes in the lack of absorption or attenuation inside the sphere. Note also that for a perfectly rigid sphere, this result can be anticipated from Eq. (4) by noticing that $\iint_{S_R}\langle v_n^{(1)}(\mathbf{r}\times\mathbf{v})\rangle\, dS_R = \iint_{S_a}\langle v_n^{(1)}(\mathbf{r}\times\mathbf{v})\rangle\, dS_a$, where S_a is the surface of the particle of radius a. At the interface fluid-rigid surface, there is absence of oscillatory movement because the sphere is considered perfectly rigid. Hence, the normal component of the fluid particle velocity $v_n^{(1)}|_{r=a} = 0$, and the torque vanishes subsequently.

III. NUMERICAL RESULTS AND DISCUSSION

The theoretical analysis performed in the previous section in a nonviscous fluid reveals the lack of the axial radiation torque in the ideal case of no absorption inside the spherical target [i.e., Eq. (18)]. In practice, common materials absorb a portion of the acoustic energy differently, and this is sufficient to produce an axial radiation torque and spin the particle.

For example, plastics and polymers, such as polyethylene (PE), phenolic polymer (PP), or polymethyl-metacrylate (PMMA) absorb a significant portion of the acoustic energy [41,42]. For the purpose of this study, a viscoelastic PE spherical shell of outer radius a and inner radius b is chosen to illustrate the theory, though other types of viscoelastic materials may be selected. The shell's material parameters are the mass density $\rho = 957$ kg/m^3, the longitudinal and shear wave velocities $c_L = 2430$ m/s and $c_S = 950$ m/s, and their corresponding normalized absorption coefficients $\gamma_L = 0.0074$ and $\gamma_S = 0.022$. The relative thickness b/a corresponds to the ratio of the inner-to-outer radii. It is used here to identify the scatterer as a sphere (i.e., $b/a = 0$), or thick (i.e., $b/a = 0.5$), thin (i.e., $b/a = 0.9$), and very thin (i.e., $b/a = 0.99$) shell. The expressions for the scattering coefficients $A_n(ka) = (\alpha_n + i\beta_n)$ for spherical shells are well-known from earlier reports on sound scattering [43,44]. Absorption is included by the standard method of introducing complex wave numbers into the theory [45]. Incorporating complex wave numbers into the acoustic scattering theory holds only for linear viscoelasticity. Here the normalized absorption coefficients of compressional and shear waves are considered constant quantities independent of frequency, an assumption that holds for PE and various other polymers [41,42].

Figure 1 shows the computations for the dimensionless axial ART resulting from the interaction of a first-order ($m = 1$) Bessel vortex beam of progressive waves with a viscoelastic PE shell filled with air ($\rho_{\mathrm{air}} = 1.23$ kg/m^3, $c_{\mathrm{air}} = 340$ m/s) in nonviscous water ($\rho_{\mathrm{water}} = 1000$ kg/m^3, $c_{\mathrm{water}} = 1500$ m/s), based on Eq. (14). The relative thickness b/a is varied from 0 to 0.99 as noted in Figs. 1(a)–1(d). The 2D plots are evaluated in the bandwidths $0 < ka \leqslant 5$ and $0^\circ \leqslant \beta \leqslant 90^\circ$. As noted from those plots, the dimensionless axial ART exhibits positive variations determined by the value of b/a. As it increases, the region corresponding to resonance peaks of high amplitudes [i.e. the "island" around $ka \sim 1.23$ and $30^\circ \leqslant \beta \leqslant 60^\circ$ for the sphere case in Fig. 1(a)] appears to shift to lower ka values.

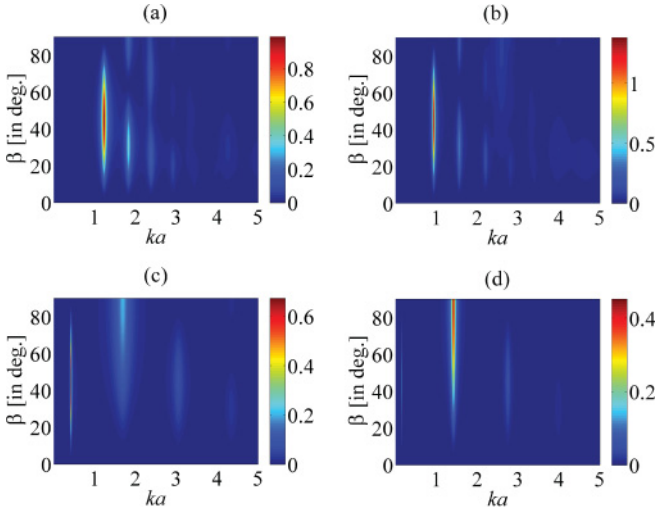

FIG. 1. (Color online) The 2D plots of the dimensionless axial ART for a first-order ($m = 1$) Bessel vortex beam of progressive waves. In this example, the viscoelastic PE shell is filled with air. In (a), (b), (c), and (d) the relative shell's thickness b/a takes the values of 0, 0.5, 0.9, and 0.99, respectively.

Differences in the dimensionless axial ART amplitude occur when the interior fluid filling the hollow core of the viscoelastic PE shell is changed to water, as shown in Fig. 2. Visual comparison of those figures shows that the torque is affected by the type of fluid filling the inner core, especially for thin (c) and very thin (d) shells.

The effect of varying the order of the Bessel vortex beam is also investigated and the results for the dimensionless axial torque for a second-order ($m = 2$) Bessel vortex beam are shown in Figs. 3 and 4 for shells filled with air or water, respectively. Comparison of Figs. 3 and 4 with Figs. 1 and 2 reveals that the torque is also affected by the order of the beam. As shown therein, the amplitude of the dimensionless axial ART is not necessarily smaller as the order of the beam increases. Those plots suggest that beams with a higher order may be more efficient for generating torques on spheres and

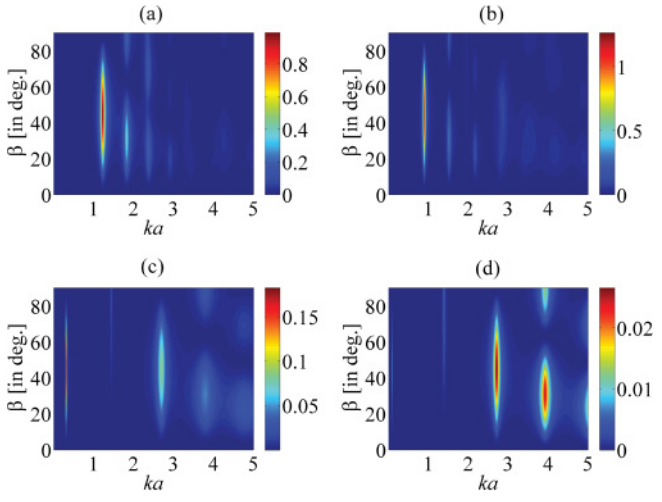

FIG. 2. (Color online) The same as in Fig. 1 but the inner core fluid is water. In (a), (b), (c), and (d) the relative shell's thickness b/a takes the values of 0, 0.5, 0.9, and 0.99, respectively.

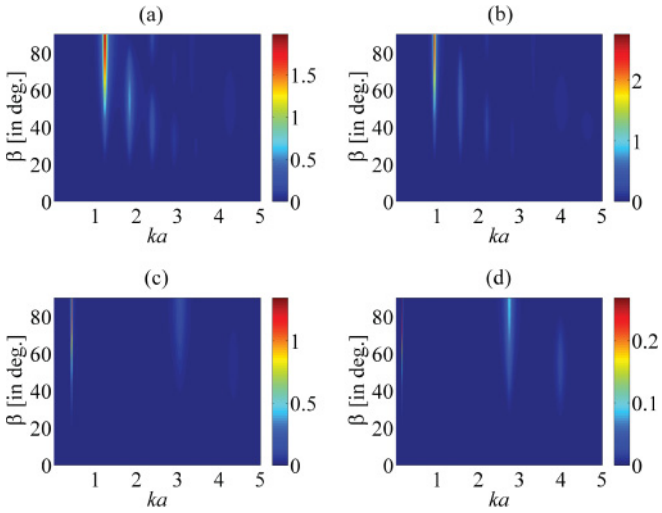

FIG. 3. (Color online) The same as in Fig. 1 but the Bessel vortex beam is of second order ($m = 2$). In (a), (b), (c), and (d) the relative shell's thickness b/a takes the values of 0, 0.5, 0.9, and 0.99, respectively.

shells should some conditions related to the frequency and the half-cone angle are met. Those conditions may be anticipated from the analytical model presented in this paper.

Additional computations have been performed to investigate the fluid-loading effect on the dimensionless axial ART for a first-order ($m = 1$) Bessel vortex beam. Figures 5 and 6 show the results for viscoelastic PE spheres (a) and shells [(b)–(d)] immersed in mercury ($\rho_{\text{mercury}} = 13600$ kg/m^3, $c_{\text{mercury}} = 1407$ m/s), a fluid with high density, and filled with air or water, respectively. From those plots it appears that the surrounding fluid with high density strongly affects the ART amplitude. A shift in the resonance peaks to lower ka values is noted for the case of spheres, thick and thin shells [(a)–(c)]. For thin shells it appears that the positions of the resonance peaks are not strongly affected by the loading effect of the

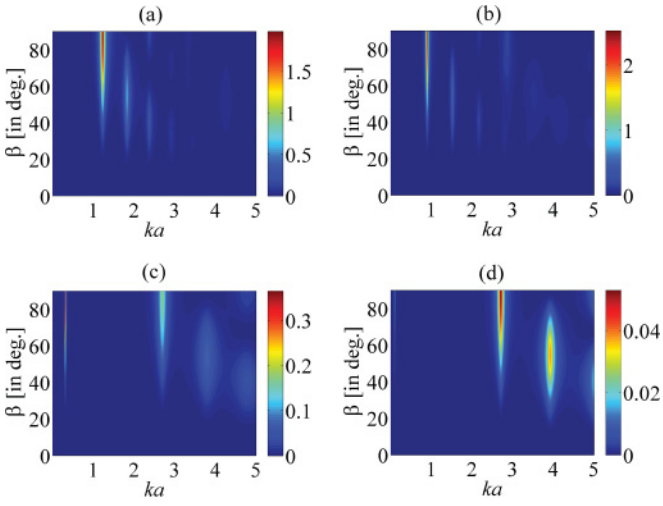

FIG. 4. (Color online) The same as in Fig. 2 but the Bessel vortex beam is of second order ($m = 2$). In (a), (b), (c), and (d) the relative shell's thickness b/a takes the values of 0, 0.5, 0.9, and 0.99, respectively.

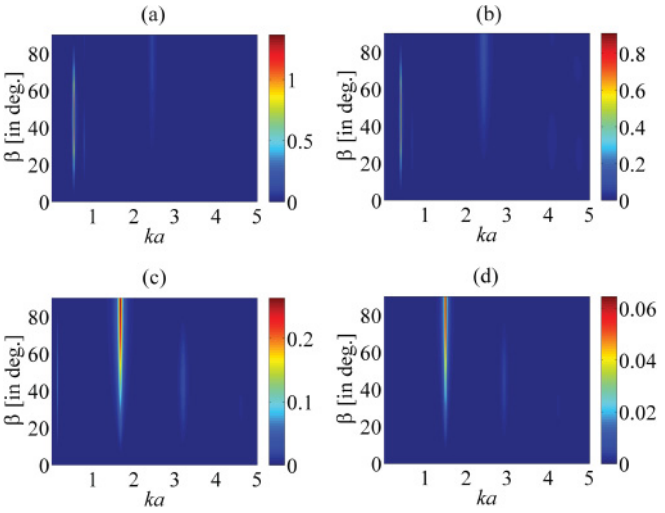

FIG. 5. (Color online) The same as in Fig. 1 but the outer fluid surrounding the spherical target is mercury. In (a), (b), (c), and (d) the relative shell's thickness b/a takes the values of 0, 0.5, 0.9, and 0.99, respectively.

surrounding fluid, however, one notices the reduction in the ART amplitude [especially Figs. 1 and 2(d) versus Figs. 5 and 6(d)].

The transition behavior of a first-order ($m = 1$) Bessel vortex beam from a progressive to a pure standing wave field is investigated by varying the ratio $0 \leqslant (\frac{|\Phi_1|}{|\Phi_0|}) \leqslant 1$ in Eq. (12). Figure 7 shows the plots for a viscoelastic PE sphere at $\beta = 50^\circ$ in the range $0 \leqslant ka \leqslant 2$ placed at an antinode in the sonic field (i.e., $h = 0$). It is interesting to note the variation in the dimensionless axial ART amplitude for each resonance peak shown in that ka bandwidth; for the resonance peak centered around $ka \sim 1.23$, the amplitude increases for the quasistanding wave behavior, to reach a maximum when the acoustic field corresponds to a pure standing wave, that is, $(\frac{|\Phi_1|}{|\Phi_0|} = 1)$. This is not the case for the resonance peak

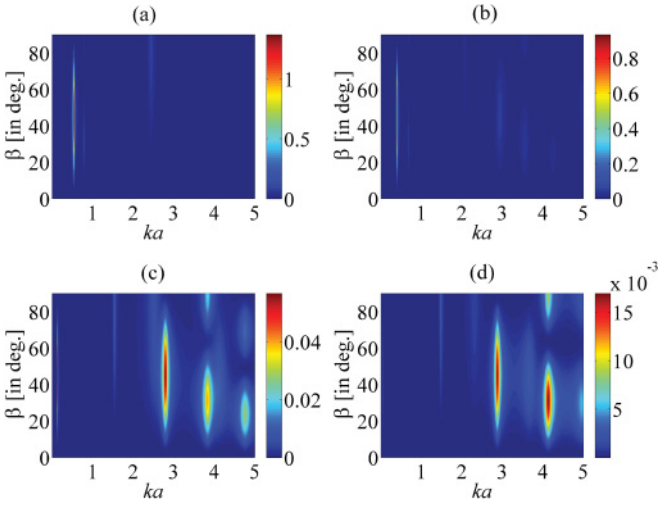

FIG. 6. (Color online) The same as in Fig. 2 but the outer fluid surrounding the spherical target is mercury. In (a), (b), (c), and (d) the relative shell's thickness b/a takes the values of 0, 0.5, 0.9, and 0.99, respectively.

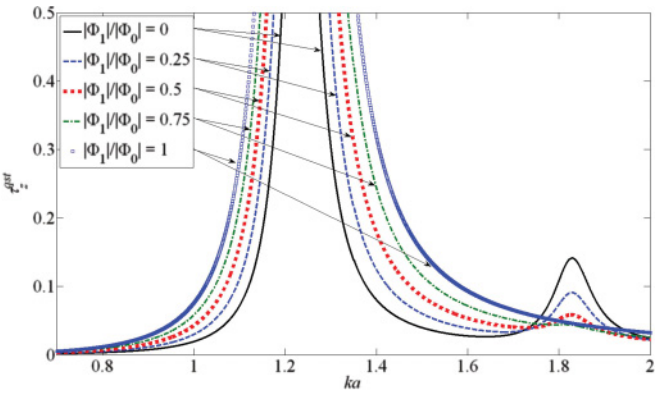

FIG. 7. (Color online) The transition behavior of a first-order ($m = 1$) Bessel vortex beam from a progressive ($|\Phi_1|/|\Phi_0| = 0$; solid line) to a pure standing wave field ($|\Phi_1|/|\Phi_0| = 1$; blue square) for a viscoelastic PE sphere (i.e., $b/a = 0$) in water. The half-cone angle is $\beta = 50^\circ$.

centered around $ka \sim 1.83$ for which the dimensionless axial ART amplitude reaches a maximum when the acoustic field corresponds to a *progressive* wave, that is, $(\frac{|\Phi_1|}{|\Phi_0|} = 0)$.

In recent works, a new type of Bessel beams has been introduced and termed therein as a higher-order Bessel *trigonometric* beam [46,47], in contrast to its vortex counterpart. Such a beam does not induce a radiation torque because it has an azimuthal dependency in the form of $\cos(m\phi)$. The surface integration according to Eq. (10) for this type of beams leads to a zero radiation torque as required by symmetry.

Previous studies on spherical and cylindrical targets [48,49] have shown that the effect of superimposing two waves propagating in perpendicular directions can produce a time-averaged ART on the particle. Balanced by the drag torque, the particle rotates with a uniform angular velocity. The mechanism for creating the ART in that case is closely connected with thermoviscous effects and absorption occurring inside the viscous boundary layer. However, the mechanism of ART production in that case differs from the case here where the ART of Bessel vortex beams is independent from the boundary layer thickness, and is present because of the effect of viscoelasticity inside the material, though the spherical particle is immersed in an ideal (nonviscous) fluid.

Concerning the question of the ART when the sphere is placed off the axis of a Bessel vortex beam, it is important to note the quantitative analyses in which the scattering on and off axis is investigated in both the near- and far-field regions for various half-cone angle and beam order values, both in acoustics [23] and optics [50]. The analyses for the off-axial scattering are important and will be used in a forthcoming investigation for the analysis of the off-axial ART.

Adding to this, is the case of the Rayleigh torque that may occur on an asymmetric object [51]. The analysis to evaluate the ART in this case requires first solving for the arbitrary acoustic scattering of a Bessel vortex beam incident upon a particle of arbitrary shape. A seminal work in electromagnetism exists [52] and could be extended to the field of acoustics, and will be the subject of a future investigation.

Similarly to the sphere's rotation driven by the *optical* axial radiation torque [53], the axial ART induces angular

acceleration of the absorbing spherical target. From Newton's second-law of motion, the angular acceleration is given by

$$\dot{\omega}_z = \frac{15E_0}{8\rho a^2}\tau_z. \tag{19}$$

When the surrounding fluid is considered viscous, the axial component of the angular velocity $\omega_z^{\rm st}$ reaches a steady value when the axial ART is balanced by an axial viscous drag torque (p. 65 in Ref. [54]),

$$N_z^d = -8\pi\eta a^3\omega_z^{\rm st}, \tag{20}$$

where η is the viscosity of the fluid, such that

$$\dot{\omega}_z + N_z^d = 0. \tag{21}$$

Upon the substitution of Eqs. (19) and (20) into Eq. (21), the axial component of the angular velocity is found to be

$$\omega_z^{\rm st} = \frac{E_0}{8\eta M}\tau_z, \tag{22}$$

where M is the moment of inertia of the sphere.

An important application of the present theory follows immediately from Eq. (22), which is the inverse characterization of the fluid viscosity from the sphere's rotation.

After submission of this manuscript for publication, another paper on the angular momentum flux of nonparaxial acoustic vortex beams and torques on axisymmetric objects has been published [55]. The axial ART on an axisymmetric object caused by a vortex wave is given by Eq. (10) in Ref. [55] as

$$\langle N_z\rangle = \frac{m}{\omega}P_{\rm abs}^{\rm pr}, \tag{23}$$

where $P_{\rm abs}^{\rm pr}$ is the absorbed power by the object. For the case of a progressive wave acoustical Bessel vortex beam incident on a sphere, as explained in Ref. [55], $P_{\rm abs}^{\rm pr}$ is given by Eq. (18) of [56] in terms of the scattering function S_n [i.e., Eq. (17) of the present paper] as

$$P_{\rm abs}^{\rm pr} = \pi c_0 E_0 \frac{1}{k^2}\sum_{n=|m|}^{\infty}\left\{(1-|S_n|^2)(2n+1) \times \frac{(n-m)!}{(n+m)!}P_n^m(\cos\beta)^2\right\}. \tag{24}$$

Upon the substitution of Eq. (24) into Eq. (23) using Eq. (17), it can be easily verified that the final result for the dimensionless axial ART is equivalent to the one given by Eq. (14).

Following a similar procedure based on Eq. (9) in Ref. [55], one can derive the absorbed power by the spherical target placed in the field of an acoustical Bessel vortex beam of quasistanding waves, such that

$$\begin{aligned} P_{\rm abs}^{\rm qst} &= \pi c_0 E_0 \frac{1}{k^2}\sum_{n=|m|}^{\infty}\left\{\left[1+\frac{|\Phi_1|^2}{|\Phi_0|^2}+2(-1)^n\frac{|\Phi_1|}{|\Phi_0|} \times \cos(2kh\cos\beta)\right](1-|S_n|^2)(2n+1) \times \frac{(n-m)!}{(n+m)!}P_n^m(\cos\beta)^2\right\}, \\ &= \frac{-4\pi c_0 E_0}{k^2}\sum_{n=|m|}^{\infty}\left\{\left[1+\frac{|\Phi_1|^2}{|\Phi_0|^2}+2(-1)^n \times \frac{|\Phi_1|}{|\Phi_0|}\cos(2kh\cos\beta)\right](\alpha_n+\alpha_n^2+\beta_n^2) \times (2n+1)\frac{(n-m)!}{(n+m)!}P_n^m(\cos\beta)^2\right\}. \end{aligned} \tag{25}$$

The standing wave case for the absorbed power $P_{\rm abs}^{\rm pr}$ follows immediately from Eq. (25) by allowing $\Phi_1 = \Phi_0$.

IV. CONCLUSIONS

The present analysis shows that an acoustical Bessel vortex beam induces an axial ART on viscoelastic spheres and shells centered on its axis of wave propagation. The analysis uses closed-form series expansions of the scattering [26] and scattering coefficients [44] for spheres and shells in Bessel vortex beams. The axial ART is caused because of sound absorption inside the particle's material and vanishes in the absence of attenuation, consistent with previous studies of electromagnetic beams [53,57]. The ART is also proportional to the order of the beam and the type of acoustic field (progressive, quasistanding, or standing wave field). Moreover, the axial ART reverses sign when the beam reverses its handedness (or helicity). Potential applications are in particle rotation and manipulation. Other applications, such as the characterization of fluids by remote measurement of angular acceleration or velocity from radiation torque induced rotation of particles and containerless processing may benefit from the analysis developed here.

ACKNOWLEDGMENTS

F.G.M. acknowledges the financial support provided through a Director's fellowship (LDRD-X9N9, Project No. 20100595PRD1, approved under LA-UR 12-10323) from the Los Alamos National Laboratory. G.T.S. and T.P.L. acknowledge CAPES PNPD-2163/2009 and CNPq (Brazilian agencies) for financial support.

[1] R. Klima and V. A. Petrzilka, Ann. Phys. **92**, 395 (1975).
[2] G. R. Torr, Am. J. Phys. **52**, 402 (1984).
[3] A. Ashkin, Phys. Rev. Lett. **24**, 156 (1970).
[4] S. Chu, Rev. Mod. Phys. **70**, 685 (1998).
[5] A. Ashkin, Proc. Natl. Acad. Sci. USA **94**, 4853 (1997).
[6] A. Ashkin and J. M. Dziedzic, Appl. Phys. Lett. **24**, 586 (1974).
[7] J. Guck, R. Ananthakrishnan, H. Mahmood, T. J. Moon, C. C. Cunningham, and J. Käs, Biophys. J. **81**, 767 (2001).
[8] A. M. Yao and M. J. Padgett, Adv. Opt. Photon. **3**, 161 (2011).

[9] S. Parkin *et al.*, in *Laser Manipulation of Cells and Tissues*, edited by M. W. B. a. K. O. Greulich (Academic, New York, 2007), p. 525.
[10] S. K. Mohanty and P. K. Gupta, in *Laser Manipulation of Cells and Tissues*, edited by M. W. B. a. K. O. Greulich (Academic, New York, 2007), p. 563.
[11] F. G. Mitri, IEEE Trans. Ultrason. Ferroelectr. Freq. Control **58**, 662 (2011).
[12] B. T. Hefner and P. L. Marston, J. Acoust. Soc. Am. **106**, 3313 (1999).
[13] J. L. Thomas and R. Marchiano, Phys. Rev. Lett. **91**, 244302 (2003).
[14] J. Lekner, J. Acoust. Soc. Am. **120**, 3475 (2006).
[15] J. Lekner, Phys. Rev. E **75**, 036610 (2007).
[16] K. Volke-Sepulveda, A. O. Santillan, and R. R. Boullosa, Phys. Rev. Lett. **100**, 024302 (2008).
[17] G. Maidanik, J. Acoust. Soc. Am. **30**, 620 (1958).
[18] W. E. Smith, Aust. J. Phys. **25**, 275 (1972).
[19] S. M. Hasheminejad and R. Sanaei, J. Comput. Acoust. **15**, 377 (2007).
[20] Z. Fan, D. Mei, K. Yang, and Z. Chen, J. Acoust. Soc. Am. **124**, 2727 (2008).
[21] D. McGloin and K. Dholakia, Contemp. Phys. **46**, 15 (2005).
[22] F. G. Mitri, Ann. Phys. **323**, 2840 (2008).
[23] F. G. Mitri and G. T. Silva, Wave Motion **48**, 392 (2011).
[24] P. L. Marston, J. Acoust. Soc. Am. **124**, 2905 (2008).
[25] F. G. Mitri, IEEE Trans. Ultrason. Ferroelectr. Freq. Control **56**, 1059 (2009).
[26] F. G. Mitri, Eur. Phys. J. E **28**, 469 (2009).
[27] F. G. Mitri, J. Phys. A: Math. Theor. **42**, 245202 (2009).
[28] P. L. Marston, J. Acoust. Soc. Am. **125**, 3539 (2009).
[29] K. Volke-Sepulveda, V. Garcés-Chávez, S. Chávez-Cerda, J. Arlt, and K. Dholakia, J. Opt. B **4**, S82 (2002).
[30] P. L. Marston and L. K. Zhang, in *Optical Trapping Applications*, OSA Technical Digest (Optical Society of America, Washington, DC, 2009), p. OMB5.
[31] L. K. Zhang and P. L. Marston, J. Acoust. Soc. Am. **129**, 2381 (2011).
[32] L. Paterson, M. P. MacDonald, J. Arlt, W. Sibbett, P. E. Bryant, and K. Dholakia, Science **292**, 912 (2001).
[33] J. P. Shelby and D. T. Chiu, Lab Chip **4**, 168 (2004).
[34] J. Friend and L. Y. Yeo, Rev. Mod. Phys. **83**, 647 (2011).
[35] X. Chen and R. E. Apfel, J. Acoust. Soc. Am. **99**, 713 (1996).
[36] G. B. Arfken and H. J. Weber, *Mathematical Methods for Physicists* (Academic, San Diego, CA, 2005).
[37] F. G. Mitri, Ann. Phys. **323**, 1604 (2008).
[38] F. G. Mitri and Z. E. A. Fellah, IEEE Trans. Ultrason. Ferroelectr. Freq. Control **55**, 2469 (2008).
[39] http://mathworld.wolfram.com/AssociatedLegendrePolynomial.html.
[40] L. Flax, G. C. Gaunaurd, and H. Uberall, Phys. Acoust. **15**, 191 (1981).
[41] B. Hartmann and J. Jarzynski, J. Appl. Phys. **43**, 4304 (1972).
[42] B. Hartmann and J. Jarzynski, J. Acoust. Soc. Am. **56**, 1469 (1974).
[43] G. C. Gaunaurd and M. F. Werby, J. Acoust. Soc. Am. **89**, 1656 (1991).
[44] G. C. Gaunaurd and M. F. Werby, J. Acoust. Soc. Am. **90**, 2536 (1991).
[45] R. H. Vogt, L. Flax, L. R. Dragonette, and W. G. Neubauer, J. Acoust. Soc. Am. **57**, 558 (1975).
[46] F. G. Mitri, J. Appl. Phys. **109**, 014916 (2011).
[47] F. G. Mitri, J. Sound Vib. **330**, 6053 (2011).
[48] F. H. Busse and T. G. Wang, J. Acoust. Soc. Am. **69**, 1634 (1981).
[49] A. Y. Rednikov, N. Riley, and S. S. Sadhal, J. Fluid Mech. **486**, 1 (2003).
[50] F. G. Mitri, IEEE Trans. Antennas Propag. **59**, 4375 (2011).
[51] J. W. S. Rayleigh, Philos. Mag. **14**, 186 (1882).
[52] J. P. Barton and D. R. Alexander, J. Appl. Phys. **69**, 7973 (1991).
[53] P. L. Marston and J. H. Crichton, Phys. Rev. A **30**, 2508 (1984).
[54] L. D. Landau and E. M. Lifshitz, *Fluid Mechanics*, Vol. 6 (Butterworth-Heinemann, London, 1987).
[55] L. K. Zhang and P. L. Marston, Phys. Rev. E **84**, 065601 (2011).
[56] L. K. Zhang and P. L. Marston, Phys. Rev. E **84**, 035601 (2011).
[57] J. P. Barton, D. R. Alexander, and S. A. Schaub, J. Appl. Phys. **66**, 4594 (1989).